ACS APPLIED MATERIALS & INTERFACES

www.acsami.org

Research Article

Accelerating Solid/Liquid Chemical Exchange-Based Isotope Separation by the Dissolution/Precipitation Mechanism

Yuchen Yang,[‖] Tye Milazzo,[‖] Wenbo Bao, Zhihao Yang, Yihan Li, Yeshiyuan Zhou, Zhihao Xu, Jinkai Si, Joseph Francis Wild, Heng Chen,* Tengfei Luo,* Alex N. Halliday,* and Yuan Yang*

Cite This: https://doi.org/10.1021/acsami.5c13443

Read Online

ACCESS | Metrics & More | Article Recommendations | Supporting Information

ABSTRACT: Isotope separation is essential for cutting-edge developments in sustainability, health, and fundamental sciences. Chemical exchange-based isotope separation (CEIS) is a scalable approach that stems from the isotope-dependent free energy of chemicals, which has already been commercialized for H/D and $^{6/7}$Li separation. However, existing CEIS processes often involve toxic materials such as H_2S and Li_xHg amalgam. Environmentally benign and low-cost materials and techniques are urgently needed to develop scalable isotope separations. CEIS processes are often between liquids and gases. Solids are attractive due to their high concentration of the nuclide of interest and the wide tunability of free energy at low temperatures. However, isotope diffusion is sluggish in most solids, making the time for isotope exchange impractical. Here we report a new exchange strategy based on accelerated dissolution/precipitation of solids in liquids where the exchange is not limited by solid diffusion. An attractive isotope separation factor of 1.021−1.026 is achieved within 10 min between solid LiCl and LiCl solution in acetone at 2 °C, which aligns with the prediction from the first-principle simulation. These results open new possibilities for scalable isotope separation between solids and liquids.

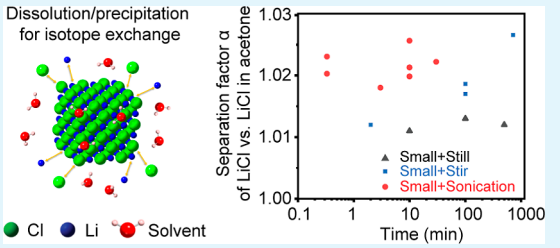

KEYWORDS: *isotope separation, nuclear fusion, chemical exchange, molecular dynamics, machine learning potential, lithium*

1. INTRODUCTION

Isotope separation and enrichment is essential for providing nuclides for cutting-edge developments in sustainability, health and fundamental sciences,[1] such as deuterium and ^{6}Li for nuclear fusion reactors,[2] ^{37}Cl and ^{7}Li for nuclear fission reactors,[3] ^{18}O, ^{68}Zn, ^{98} Mo, ^{176}Yb as medical radioisotope precursors for medical imaging and cancer treatments,[4] ^{48}Ca for creating superheavy elements,[5,6] and ^{28}Si for quantum computing.[1,7]

While various methods have been developed for isotope enrichment, such as gas centrifugation and electromagnetic (EM) separation,[8−13] they often face challenges of high cost, low productivity, and high toxicity.[1] For example, gas centrifugation often uses highly toxic precursors (e.g., UF_6 for $^{235}U/^{238}U$), and EM separation has an extremely low production rate of grams per year. Chemical exchange is an attractive alternative because it can operate at near-ambient conditions and is easy to scale up. Chemical exchange is based on the isotope mass-dependent atomic vibration and thus Gibbs free energy (G), leading to the enrichment of an isotope in one phase when two phases are in contact. The corresponding separation capability is often evaluated by the separation factor (α), which is defined as the ratio of isotope ratios in two phases $([A^*]/[A])_1/([A^*]/[A])_2$. One and 2 refer to two phases, and [A] and [A*] mean the concentration of isotopes A and A*, respectively. According to chemical equilibrium, we have

$$\alpha = \frac{([A^*]/[A])_1}{([A^*]/[A])_2} = \exp\left[-\left(\frac{G_{A^*,1} - G_{A,1}}{RT} - \frac{G_{A^*,2} - G_{A,2}}{RT}\right)\right] = \exp\left[-\frac{\Delta G_1 - \Delta G_2}{RT}\right] \quad (1)$$

where R is the ideal gas constant, and T is the temperature.

Chemical exchange-based isotope separation (CEIS) is mainly used for light isotopes since $\alpha \propto (m^* - m)/m/m^*$, where m is the mass of an isotope.[14] CEIS is often performed in the form of gas/gas, gas/liquid, and liquid/liquid due to their fast exchange kinetics, such as H_2S/H_2O for H/D separation (Girdler process)[15] and Li_xHg (liquid)/LiOH (aq) for $^{6/7}$Li separation (COLEX process).[16] Crown ether-based liquid/liquid exchange has also been explored for Li, Ca, and other isotopes.[17−20] Although reasonable α can be achieved,

Received: July 8, 2025
Revised: November 3, 2025
Accepted: November 5, 2025

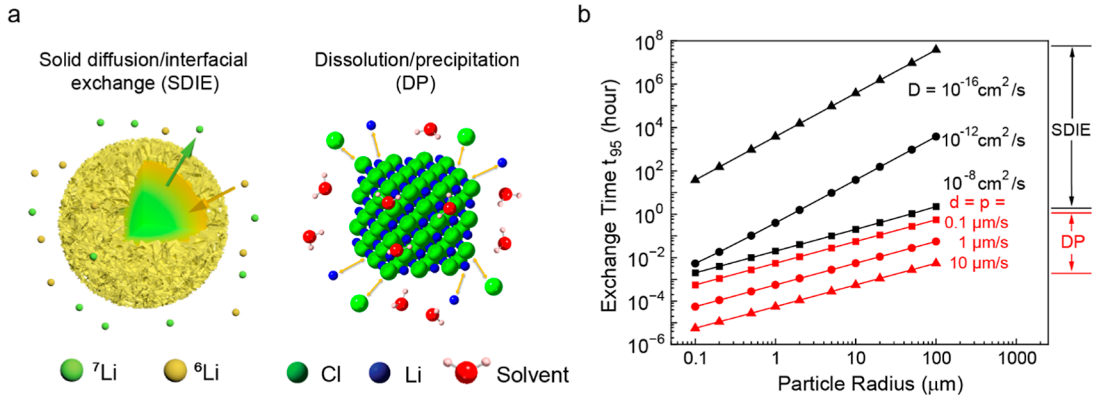

Figure 1. (a) Schematics of two isotope exchange mechanisms between a solid and a liquid. Left: solid diffusion/interfacial exchange (SDIE). Right: dissolution/precipitation (DP). (b) The exchange time vs particle radius by the two mechanisms above: (1) solid diffusion and interfacial exchange (black lines). (2) dissolution/precipitation (red lines). The exchange time (t_{95}) is defined as the time taken to reach 95% of equilibrium isotopic ratios (t_{95}).

such as 1.32 for H_2S/H_2O, 1.05 for Li_xHg (liquid)/LiOH (aq), 1.02−1.06 for crown ethers ($^{6/7}$Li), and 1.010 for ($^{40/48}$Ca),[14,21−23] they often include toxic materials (e.g., H_2S, Hg), or have low distribution factors and high costs (e.g., crown ethers).[17]

CEIS also exists between a solid and a liquid, which has the following potential advantages: (1) the concentration of an element in solids can easily reach >10 M, which makes the exchange system compact and reduces the cost. (2) The operating temperature can be low, which favors a large α since α scales with $1/T$.[2,24,25] (3) Solids are diversified in terms of bonding, providing a versatile pool for maximizing α.

CEIS in solid/liquid systems has been widely observed in geochemical processes with noticeable α, such as Li minerals vs Li^+ ions in water for $^{6/7}$Li,[26−28] and Mg calcite vs Mg^{2+} ions in water for $^{24/26}$ Mg,[29,30] and α typically ranges from ∼1.001 to 1.03 in these natural processes. However, solid/liquid exchange is rarely explored for intentional isotope separation. One main reason is the time scale to reach isotope equilibrium in geographical processes (e.g., days and years[29,31,32]), which is not acceptable for scalable isotope production since tens or hundreds of steps in a cascade are needed for enrichment to the target abundance.[33] Moreover, even for solids with fast isotope exchange, the interconversion between solid and liquid is also not easy to realize, which is needed to complete the loop of enrichment.[34]

In this paper, we propose a new dissolution/precipitation process to overcome such kinetic barriers and enable fast isotope exchange between solids and liquids. Isotope exchange is achieved by solid dissolution and precipitation from a saturated liquid solution, and thus, the exchange is no longer limited by the sluggish diffusion in solids. Moreover, we find that moderate stirring and sonication can accelerate the exchange rate by 1−2 orders of magnitude. With this combined strategy, the time to complete the exchange is reduced to minutes. Specifically, we have achieved α of 1.021−1.026 for $^{6/7}$Li by sonicating LiCl solid in a solution of LiCl in acetone at 2 °C within 10 min, and α of 1.015−1.017 by cooling saturated LiBr in water from 22 to 2 °C within 10 min. These results are consistent with first-principle simulations. Further materials optimization could enhance α and lead to practical systems for scalable isotope separation.

2. DESIGN PRINCIPLES

As shown in Figure 1a, there are two main mechanisms to realize isotope exchange between a solid and a liquid: (1) solid diffusion and interfacial exchange (SDIE), where atoms in a solid diffuse to the solid/liquid interface, followed by an interfacial exchange with a liquid. The isotope exchange time is limited by solid diffusion for large particles and interfacial exchange for small particles. (2) Dissolution and precipitation (DP), where a solid is dissolved in a liquid and reprecipitated. The isotope exchange time is limited by the dissolution/precipitation rate.

Figure 1b shows the time to complete 95% of isotope exchange (t_{95}) in both SDIE and DP mechanisms. In SDIE, we assume a moderate interfacial isotope exchange rate of 10^{-4} mol/m^2/s (see Supporting Information Section 1.2). Under a diffusivity (D) of 10^{-8} cm^2/s, which represents good solid ionic conductors,[35] t_{95} is 0.6 min for particle radius r = 1 μm, and 8 min for r = 10 μm. This is fast enough, but good solid ionic conductors are very limited.[36] When D is 10^{-12} cm^2/s, which represents common ionic conductors (e.g., Li_xC, $LiINi_xMn_yCo_{1-x-y}O_2$), t_{95} increases to 25 min for r = 1 μm, and 700 min for r = 10 μm, which are long for scalable isotope separation. Figure 1b also shows that SDIE is impractical for plenty of chemicals where ions are nearly immobile inside (e.g., most salts and oxides, for which $D < 10^{-16}$ cm^2/s). When D is 10^{-16} cm^2/s, t_{95} is 38 h for r = 100 nm and 3 h for r = 10 nm.

On the other side, the isotope exchange time for the DP mechanism (t_{DP}) is determined by the dissolution rate of a solid (d) and the precipitation rate from the liquid (p). They both have the unit of m/s, which means the thickness of solid dissolved and precipitated per second, respectively. Therefore, $t_{dp} = r\left(\frac{1}{d} + \frac{1}{p}\right)$. While both d and p depend on solute concentration in the liquid phase, experiments show that common readily soluble salts have d and p on the order of ∼0.001−0.1 μm/s without stirring, ∼0.1−1 μm/s with stirring, and ∼1−10 μm/s using sonication, at least semiquantitatively (Figure S2). Therefore, with sonication, the time scale to realize complete isotope exchange could be ∼1 min even for large particles with r = 10−100 μm (Figure 1b), which is much faster than SDIE. Such a time scale is attractive for large-scale isotope separation.

https://doi.org/10.1021/acsami.5c13443
ACS Appl. Mater. Interfaces XXXX, XXX, XXX−XXX

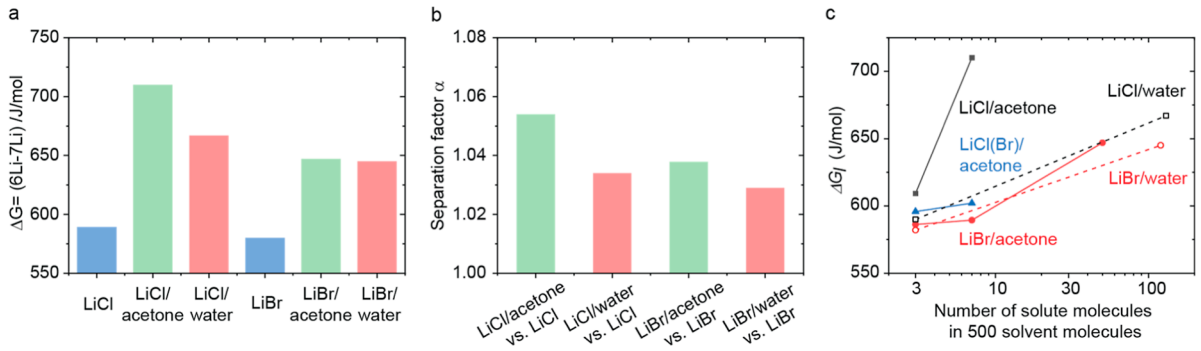

Figure 2. (a) ΔG ($=G_{6Li} - G_{7Li}$) of solid LiCl, solid LiBr, and saturated solutions of LiCl and LiBr in acetone and water. The values of solids are calculated by DFT, and the values of liquids are calculated by PIMD (see Section 2 in Supporting Information). (b) The computed separation factor α based on the result in (a). (c) The dependence of ΔG_l on different solute-to-solvent ratios. The number of solvent molecules in each simulation is fixed at 500.

To demonstrate that the proposed dissolution/precipitation mechanism can accelerate isotope exchange between a solid and a liquid, we have selected $^{6/7}$Li as a model system since low-mass isotopes favor high α, and both isotopes are critical to nuclear fusion and fission reactors.[2,3] To facilitate scalable production, we particularly focus on low-cost and environmentally benign materials. Moreover, the solid phase should have a reasonable solubility in the liquid phase (e.g., >0.1 mol/L) to reduce the total amount of liquid. Therefore, we have selected LiCl and LiBr as two candidates for the solid phase and their saturated solutions in acetone and H_2O as candidates for the liquid phase. These selections are just to demonstrate the viability of solid/liquid exchange; the concept can be expanded to many other solids and liquids in the future.

3. MATERIALS AND METHODS

3.1. Materials. Anhydrous lithium chloride (free-flowing, Redi-Dri, ReagentPlus, ≥99%) and anhydrous lithium bromide (free-flowing, Redi-Dri, ReagentPlus, ≥99%), along with acetone (ACS reagent, ≥99.5%), were all purchased from Sigma-Aldrich. Deionized water is produced by a water purifier (Direct-Q 5UV Remote Water Purification System).

3.2. Chemical Exchange Experiments. In the exchange between LiCl solid and LiCl in acetone, 84 mg LiCl was added into 3.95 g of acetone in a polypropylene container in an ice/water bath, which forms a mixture of solid LiCl and saturated LiCl solution in acetone. The molar ratio of Li in solid and liquid is 1:1. In the exchange between LiBr solid and LiBr in acetone, 690 mg LiBr was added into 2 g of acetone in a polypropylene container, which forms a mixture of solid LiBr and saturated LiBr solution in acetone. The ratio of Li in solid and liquid is 1:1. In the exchange between LiBr solid and LiBr in water by cooling, 6.08 g of LiBr were dissolved in 3.5 g of water at room temperature in a polypropylene container, followed by cooling down in an ice/water bath.

In all experiments above, the mixture is either kept still, or under stirring, or under sonication for the target period. The sonication was performed by a BRANSON 1800 sonicator. Upon completion of chemical exchange, the mixtures were transferred to 50 mL centrifuge tubes and centrifuged at 9000 rpm for 5 min to separate solid particles and liquid (Thermo Scientific, SORVALL LEGEND X1 Centrifuge). The separated liquid and solid were then used for isotope analysis.

3.3. Material Characterization. A scanning electron microscopy (SEM; ZEISS SIGMA VP) was employed to analyze particle sizes for both LiCl and LiBr before and after ball milling. The recrystallized monohydrate of LiBr was characterized using an X-ray Diffraction (XRD; Synergy-S SCXRD) to assess crystal structure and purity.

A Nu Sapphire Multicollector Inductively Coupled Plasma Mass Spectrometry (MC-ICP−MS; SP005) was used for Li isotopic measurements. All solids were first dissolved in 10 wt % nitric acid, and then roughly diluted to solutions containing ~200 ppb Li using 2% nitric acid. Once the concentration measurements of samples had been made by comparing the ^{7}Li beam intensities of the solutions to the reference, the concentrations of all isotope samples were diluted and brought within 10% of the standard solution concentration (50 ppb). The H9 and L6 Faraday cups were used to collect ^{7}Li and ^{6}Li signals simultaneously. Isotopic measurements were then made three to six times for each sample, and each measurement consisted of 50 cycles of 3 s integrations. Every isotope sample and Li standard solution were measured alternately, so that mass bias and signal drift with time could be accounted for.

3.4. MD and DFT-Based Simulation of Isotope Separation. Molecular dynamics (MD) simulations were performed to help validate results and discover trends between varying characteristics. Simulations focused on three solvents: LiF, LiCl, and LiBr. These solvents are mixed with acetone and either isotope ^{6}Li or ^{7}Li. Generalized Amber Force Field (GAFF) parameters were assigned to each atom using the Maginn Force Field Archive (MAFFA).[37] MAFFA calculates and applies atomic charges using the restrained electrostatic potential (RESP) method.[37] Path integral molecular dynamics (PIMD)[38] was implemented to increase the accuracy of interactions by incorporating quantum mechanics into the MD process using large-scale atomic/molecular massively parallel simulator (LAMMPS). The free energy perturbation (FEP) of the solvents was calculated during each simulation, which was then used to calculate the finite-difference thermodynamic integration (FDTI).[39] Equilibration was done first with *NPT*, then *NVT*, and *NVE* for stability (see Supporting Information Section 2).

To calculate the FEP of the lithium isotope, a small perturbation and coupling factor to control the bonding interactions in the system was set up. The system transitions from a noninteracting system to a fully interacting one. The difference in energy between interaction states calculates FEP, which is needed to determine FDTI.

The ab initio calculations were performed using the Quantum ESPRESSO[40] package within the local-density approximations (LDA)[41] corrected by Perdew−Burke−Ernzerhof exchange−correlation functional[42] to calculate the atomic forces and extract harmonic interatomic force constants. A cutoff of the wave functions, and the convergence threshold for force and energy were set to maximize stability and select *K*-points in the first Brillouin zone (see Supporting Information 2). The phonon vibrational computations used the linear response technique based on perturbation density functional theory (DFPT).[43]

4. RESULTS

4.1. Molecular Simulations. After selecting the solid/liquid systems to investigate, we first use first-principles calculations to study if they can achieve attractive α. All simulations were made for 275 K, which is the temperature in the experiments. It is already established that first-principle

https://doi.org/10.1021/acsami.5c13443
ACS Appl. Mater. Interfaces XXXX, XXX, XXX−XXX

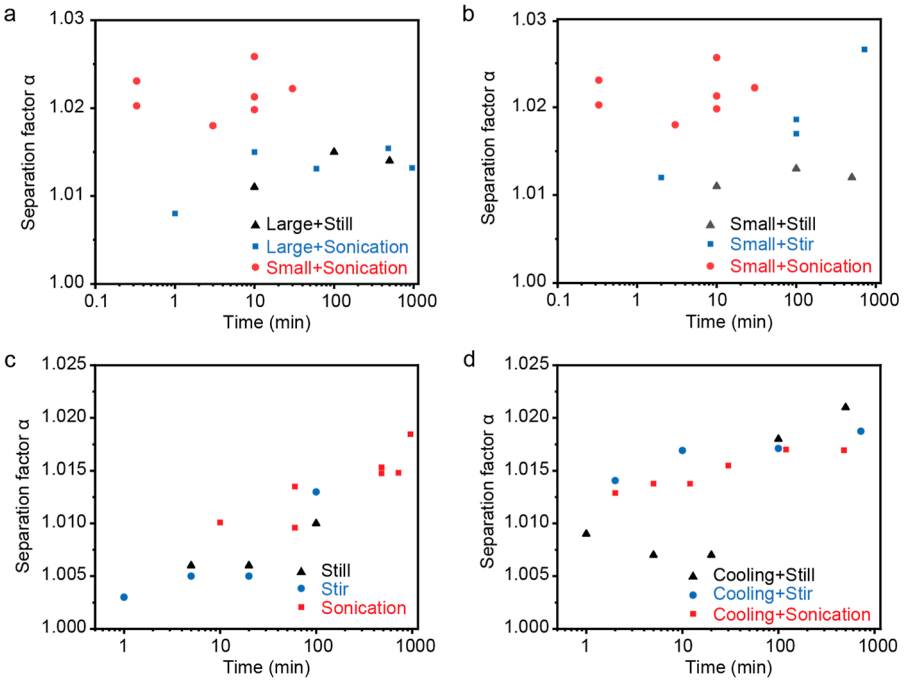

Figure 3. (a,b) The experimental separation factor α versus time in LiCl solid particles vs LiCl saturated in acetone. (a) Results of large particles without disturbance (black), large particles with sonication (blue), and small particles with sonication (red). (b) Results of small LiCl particles without disturbance (black), with stirring (blue), and with sonication (red). (c,d) Separation factor α of LiBr vs saturated LiBr in water. (c) Results of small particles without disturbance (black), with stirring (blue), and with sonication (red). (d) Results of cooling without disturbance (black), cooling with stirring (blue), and cooling with sonication (red). The temperature was cooled from 22 to 2 °C. In (a−c) the exchange temperature was maintained at 2 °C.

simulations can provide reasonable consistency with experimental observations.[44] For example, path-integral molecular dynamics (PIMD) simulations can resolve small deviations in α-for instance, a deviation of ∼0.003 for Mg calcite vs $Mg^{2+}(aq)$,[45] and an error of 0.01 in Li minerals vs $Li^{+}(aq)$.[46]

In the solid/liquid exchange of $^{6/7}Li$, eq 1 can be rewritten as

$$\alpha = \frac{([^6Li]/[^7Li])_s}{([^6Li]/[^7Li])_l} = \exp\left[-\left(\frac{G_{6Li,s} - G_{7Li,s}}{RT} - \frac{G_{6Li,l} - G_{7Li,l}}{RT}\right)\right] = \exp\left[-\frac{\Delta G_s - \Delta G_l}{RT}\right] \quad (2)$$

where the subscripts s and l correspond to solid and liquid, respectively. In solids and liquids, as different isotopes do not affect electronic interactions among atoms, the main isotope-induced difference in G is the vibrational free energy, which is mass-dependent. Based on the phonon theory, G of a crystalline solid with a pure isotope can be expressed as follows.

$$G_s = -k_B T \ln(Z) = \sum_{i=1}^{3N} \frac{\hbar\omega_i}{2} + k_B T \sum_{i=1}^{3N} \ln(1 - e^{-\hbar\omega_i/k_B T}) \quad (3)$$

where Z is the partition function, and ω_i is a vibrational mode of the solid, which can be obtained by DFT-based phonon calculations. Here, we omit the contribution of the PV term in G since it is very small for solids at the ambient pressure (∼1 J/mol), not to mention the difference caused by isotopes.

DFT results show that ΔG_s = 589 J/mol for LiCl and 580 J/mol for LiBr (Figure 2a). The positive value arises from the fact that the phonon vibrational frequencies of a chemical with ^6Li are always higher than the same chemical with ^7Li, leading to a larger G of that with ^6Li. Similarly, the slightly more positive value of ΔG_s in LiCl than in LiBr stems from the stronger isotope dependence due to higher vibrational frequencies in LiCl. But overall, the difference is not substantial since 9 J/mol only corresponds to a change of 3.9×10^{-3} in α at 275 K.

On the other hand, PIMD was used to calculate ΔG_l since nonharmonic vibration needs to be considered. As shown in Figure 2a, ΔG_l are 710 ± 1, 647 ± 2, 667 ± 3 and 645 ± 3 J/mol for saturated LiCl in acetone (0.2 M, 500:7), saturated LiBr in acetone (1.5 M, 500:50), saturated LiCl in water (16.1 M, 500:130), and saturated LiBr in water (16.5 M, 500:120), respectively. The ratios in parentheses correspond to the number of solvent molecules to salt molecules in the simulation. Therefore, the corresponding α values are 1.054, 1.039, 1.034, and 1.029 for LiCl in acetone vs LiCl solid, LiBr in acetone vs LiBr solid, LiCl in water vs LiCl solid, and LiBr in water vs LiBr, respectively (Figure 2b).

Such results show that α of LiCl in acetone vs LiCl solid is substantially higher than other combinations. To understand the underlying mechanism, we studied how ΔG_l depends on the salt concentration. As shown in Figure 2c, ΔG_l at a low concentration (solvent/solute = 500:3) has similar values for all solutions (580−610 J/mol). However, LiCl in acetone shows a steep decrease in ΔG_l compared to other situations when the salt concentration increases, even compared to LiBr in acetone, where only the anion changes. Such different concentration-dependent behavior leads to the distinct ΔG_l of LiCl in acetone at saturation.

To better understand this phenomenon, we further compared ΔG_l of LiCl, LiBr, and an artificial LiCl (Br) salt

https://doi.org/10.1021/acsami.5c13443
ACS Appl. Mater. Interfaces XXXX, XXX, XXX−XXX

at the solubility of LiCl in acetone (solvent/solute = 500:7). LiCl (Br) means that the Cl^- anion has the mass of Br^-, but the same interaction potential as Cl^-, which can help separate effects of mass and interaction potential. As shown in Figure 2c, ΔG_l of LiCl (Br) is 602 ± 1 J/mol, which is very close to the value of LiBr (589 ± 2 J/mol), but far from that of LiCl (710 ± 1 J/mol). Such results suggest that the substantially higher ΔG_l of LiCl in acetone arises from the mass effect rather than the different interaction potential between Br^- and Cl^- ions. The mass of anions may affect the vibrational spectrum in a liquid and thus ΔG_l, which requires further investigation to understand the underlying governing mechanisms.

4.2. Isotope Exchange in LiCl/LiBr Solids vs Saturated Solution in Acetone. The molecular simulation above shows that LiCl solid vs LiCl in acetone has the largest α. We further experimentally studied this system. In a typical experiment, LiCl particles are added to a saturated LiCl/acetone solution (0.2 M) at 2 °C, and the molar ratio of Li in the two phases is 1:1. After a period of time, the solid and the liquid phases are separated. Then, the $^6Li/^7Li$ ratio inside was measured by a high-resolution multicollector inductively coupled plasma mass spectrometer (MC-ICPMS) (Nu Instruments Sapphire equipped with a collision cell). The uncertainty in α is below 0.001.

We only observed α of 1.010−1.015 after mixing (black dots in Figure 3a), which are far away from the predicted value of 1.054 above. Sonication to speed up LiCl dissolution and precipitation made little difference. The measured α remained at ∼1.010−1.015 after 100−1000 min of exchange (blue dots in Figure 3a).

This difference may arise from the large size of LiCl particles (100−500 μm, Figure S6a). Calculation shows that the diffusion time of Li^+ in LiCl is significantly longer than the exchange time (see Section 3 in the Supporting Information for details). As Li^+ ions diffuse slowly in LiCl and the dissolution rate of LiCl is low in acetone, LiCl in the inner part of solid particles may not exchange with the liquid phase, which reduces α. Therefore, ball milling was deployed to reduce the size of the LiCl particles to ∼5 μm (Figure S6b). With such small LiCl particles and sonication, α rises substantially to ∼1.020−1.023 even after just 20 s of sonication and increases slightly further to 1.021−1.026 after 10−30 min of sonication. Therefore, not only α is higher than with large LiCl particles, but also this higher α is achieved much more quickly than with large LiCl particles. Therefore, reducing particle size is critical for enhancing the kinetics of isotope exchange between a solid and a liquid, which is important for scalable isotope enrichment.

We further studied the effects of mixing methods on the isotope exchange with small LiCl particles (Figure 3b). Without any disturbance, α is only 1.011, 1.012, and 1.011 after 10, 100, and 480 min, respectively, which indicates that dissolution of small LiCl particles is still inefficient without disturbance. With stirring, α reaches 1.012, 1.018, and 1.026 at 2, 100, and 480 min, respectively, which are much higher, indicating the effectiveness of stirring to enhance dissolution/precipitation kinetics. However, stirring is less efficient than sonication since α of ∼1.020 is achieved even with just 20 s of sonication. We think that this arises from the fact that sonication provides higher energy to break particles and expose new solid surfaces to speed up isotope exchange.

After understanding the effects of particle size and disturbance methods in LiCl solid vs saturated LiCl in acetone, we further tested ball-milled LiBr solid vs saturated LiBr in acetone (Figure S7). After sonicating for 5, 20, 100, and 300 min, the values of α are only 1.004, 1.004, 1.007, and 1.007, respectively. Such results indicate that LiBr solid vs saturated LiBr in acetone is not ideal for enriching lithium isotopes.

The best experimental α in above systems are both ∼0.03 lower than simulation results (1.026 vs 1.054 for LiCl/acetone vs LiCl, and 1.007 vs 1.038 for LiBr/acetone vs LiBr). This may be because of the following: (1) the solid and the liquid phases are simulated by DFT and PIMD, respectively, so there may be a systematic shift of energy between the two methods. (2) The isotope exchange between the solid and the liquid is not completed. (3) In sonication, the local temperature is higher than the environmental temperature (2 °C). Nevertheless, the simulation correctly predicted that α for LiCl/acetone vs LiCl is ∼0.02 larger than that for LiBr/acetone vs LiBr. Therefore, simulations can provide guidance to screen and predict isotope separation in solid/liquid chemical exchange. The method can be further extended to other isotopes of other elements (e.g., Ca, K).

4.3. Cooling-Induced Fast Isotope Exchange in LiCl/LiBr vs Saturated Solution in H_2O. Given the evidence of the effects of particle size and disturbance, we further explored LiBr vs LiBr in water. Although simulations show that this system has only a moderate α of 1.029, the high concentrations of Li^+ in LiBr solid (39.8 M) and saturated LiBr aqueous solution (19.2 M) make it potentially attractive for scaling up.

The first experiment mixed 6.08 g LiBr with 3.5 mL H_2O so that the molar ratio of Li^+ ions in solid to those in liquid is unity. Under sonication, α reached 1.010, 1.013, and 1.015 at 10, 60, and 500 min, respectively (Figure 3c). Surprisingly, such values are not significantly higher than α without any disturbance, which are 1.006,1.006, and 1.010 at 5, 20, and 100 min, respectively. With stirring, α gave 1.005, 1.005, and 1.013 at 5, 20, and 100 min, respectively (Figure 3c).

We attribute such weaker dependence of α on disturbance to the fact that LiBr is highly hygroscopic, so the ball-milled particles (Figure S6d) merge together quickly in air or after being immersed in water (Figure S8). Therefore, even sonication is ineffective in speeding up the dissolution of LiBr particles. This issue may also present itself in various salts with high solubility in target solvents, which is favored for scaling up.

To overcome this, we propose a strategy of cooling-induced precipitation to maximize isotope exchange between the liquid and the solid phase. In short, when the temperature decreases, LiBr becomes less soluble and precipitates out. As the growth of a solid precipitate is a layer-by-layer process starting from a nanoscale nucleus with a large surface area, the isotope exchange rate should be greatly enhanced.

To test this strategy, a saturated LiBr aqueous solution was cooled from 22 to 2 °C by placing it in an ice bath. As the solubilities of LiBr in water are 19.2 and 16.7 mol/L at 22 and 2 °C, respectively, 20% of dissolved LiBr will precipitate out during cooling. When the solution was cooled with stirring, α reached 1.014 and 1.017 quickly at 2 and 10 min, respectively, and then slowly increased to 1.017 and 1.018 at 100 and 500 min, respectively (Figure 3d). When sonication was applied during cooling, α reached 1.013, 1.013 quickly at 2 and 10 min, respectively, and kept increasing to 1.015 and 1.016 at 30 and 100 min, respectively. These values at short periods (e.g., 2 and 10 min) are substantially larger than corresponding values

https://doi.org/10.1021/acsami.5c13443
ACS Appl. Mater. Interfaces XXXX, XXX, XXX−XXX

without cooling-induced precipitation in Figure 3c. Therefore, cooling-induced precipitation is a practical strategy to further enhance isotope separation, particularly for hygroscopic salts, which tend to form large crystals in solvents.

The best experimental α of LiBr/water vs LiBr (1.019) is 0.010 lower than the simulation result (1.029). Besides the reasons discussed in the acetone systems in Section 4.2, it should be pointed out that the real solid phase involved in the exchange experiments is a mixture of $LiBr{\cdot}2H_2O$ and $LiBr{\cdot}3H_2O$ instead of LiBr (Figure S9), which aligns with the phase diagram.[47] Unfortunately, it is computationally expensive to simulate the phonon spectrum of $LiBr{\cdot}2H_2O$ and $LiBr{\cdot}3H_2O$ as they have lower symmetries and contain 8 and 11 atoms in a primitive cell, respectively. We tentatively use lattice dynamics with the Matlantis universal machine learning potential[48] to compute ΔG_s of $LiBr{\cdot}2H_2O$, which leads to an α of 1.018 for exchanging with saturated LiBr aqueous solution, aligning well with the experimental value of ~1.020 (see Section 5 in Supporting Information for more detailed discussion). In the future, we will perform more studies on simulating ΔG_s of hydrates to get more accurate results. The results above indicate that the introduction of hydrates may not significantly change α, but the consistency between experiments and simulation requires further examination. This issue also exists for LiCl, where the solid phase is $LiCl{\cdot}2H_2O$ instead of LiCl.

4.4. Multistage Demonstration and Cost Analysis. After validating $^{6/7}$Li isotope separation in a single stage, we further extend it to three stages to explore scalability. LiCl solid vs LiCl in acetone is used as an example. We started with 85 mg of ball-milled small solid LiCl in 5 mL in acetone, which is the same as that in a single-stage experiment in Figure 3b. After 30 min sonication, the δ values of $^{7/6}$Li, which is defined as the isotope ratio relative to a reference sample $[([^7Li]/[^6Li])_{sample}/([^7Li]/[^6Li])_{reference} - 1] \times 1000‰$, are $-84.7 \pm 0.5‰$ and $-64.4 \pm 0.3‰$ in the liquid and the solid phase, respectively, corresponding to an α of 1.022 ± 0.001. Then, the liquid phase enriched in ^{7}Li is extracted for the second separation. Half of the liquid was completely dried to yield solid LiCl powder, followed by mixing such solid powders with the second half of the liquid phase extracted. Therefore, in the second exchange, the initial isotope abundances and the total amount of lithium in both phases are the same. Such a process is further repeated for the third separation.

We found that α for stages 2 and 3 are 1.012 ± 0.001 and 1.016 ± 0.001, respectively (Figure 4). The lower values compared to stage 1 are likely due to the fact that LiCl solids used in stages 2 and 3 were derived from evaporation, which formed much larger crystals than ball milling. Therefore, α values are closer to those for sonicating large particles (1.01−1.015, blue dots in Figure 3a). We think that this issue can be addressed by two categories of methods: (1) using sonication or surfactant to reduce particle size during drying, and (2) designing a cascade to avoid recrystallization of solids between different stages, which is more scalable for large-scale production. The details of the cascade design are shown in Figure S3. Methods to better break solid particles should be investigated in further studies.

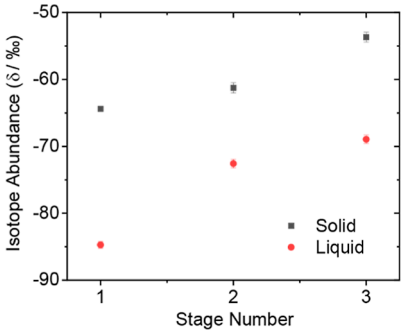

Figure 4. Isotope abundance in the solid and the liquid phases in three-stage separation. The abundance δ is defined as the relative value to the reference sample $[([^7Li]/[^6Li])_{sample}/([^7Li]/[^6Li])_{reference} - 1] \times 1000‰$.

The reported dissolution/precipitation method also has lower materials cost and better environmental friendliness than conventional COLEX and crown ether-based solvent extraction methods. As shown in Section 7 in the Supporting Information, a single-stage COLEX process with an α of 1.05 has a material cost of $245.7 K with 1 kg Li present in each phase. Similarly, a single-stage crown ether-based separation (α = 1.05) has a material cost of $30.6 K with 1 kg Li present in each phase. In contrast, as LiCl solid vs LiCl in acetone has an α of 1.025, three stages are required to achieve the same separation capability as COLEX or crown ether-based processes above. The corresponding cost including materials and electricity is $2.3 K for three stages, which is much less than the COLEX and crown ether processes. Moreover, regarding environmental friendliness, the quantity of organic solvents in the reported process is also much less than in the crown ether-based process, and no Hg is involved.

5. CONCLUSIONS

Chemical exchange is an efficient and scalable approach to separate isotopes, particularly those with low masses. Isotope separation between solid and liquid has been widely observed in natural geochemical systems, but its poor kinetics makes it largely neglected for practical large-scale isotope enrichment. In this study, we developed a dissolution/precipitation strategy, which greatly accelerates isotope separation in solid/liquid exchange down to seconds to minutes. In particular, we found that sonication and stirring are effective in reducing isotope exchange time. We achieved a separation factor α of 1.021−1.026 in LiCl solid vs saturated LiCl in acetone within 10 min under sonication and α of 1.015−1.017 within 10 min in LiBr vs saturated LiBr in water. The results also align with molecular simulations. These findings pave the way for a rational approach to search for systems with high isotope separation factors and efficient separation for scalable production.

■ ASSOCIATED CONTENT

Data Availability Statement

All data are available in the manuscript or the Supporting Information. Information requests should be directed to the corresponding authors.

Supporting Information

The Supporting Information is available free of charge at https://pubs.acs.org/doi/10.1021/acsami.5c13443.

Additional experimental details, materials, and methods. Details of isotope exchange modeling and simulations. Scale-up designs and cost analysis (PDF)

https://doi.org/10.1021/acsami.5c13443
ACS Appl. Mater. Interfaces XXXX, XXX, XXX−XXX

AUTHOR INFORMATION

Corresponding Authors

Heng Chen − *Lamont-Doherty Earth Observatory, Columbia University, Palisades, New York 10964, United States*; Email: hengchen@ldeo.columbia.edu

Tengfei Luo − *Department of Aerospace and Mechanical Engineering, University of Notre Dame, Notre Dame, Indiana 46556, United States*; orcid.org/0000-0003-3940-8786; Email: tluo@nd.edu

Alex N. Halliday − *Lamont-Doherty Earth Observatory, Columbia University, Palisades, New York 10964, United States*; Email: alexhalliday@climate.columbia.edu

Yuan Yang − *Department of Applied Physics and Applied Mathematics, Columbia University, New York, New York 10027, United States*; orcid.org/0000-0003-0264-2640; Email: yy2664@columbia.edu

Authors

Yuchen Yang − *Department of Applied Physics and Applied Mathematics, Columbia University, New York, New York 10027, United States*

Tye Milazzo − *Department of Aerospace and Mechanical Engineering, University of Notre Dame, Notre Dame, Indiana 46556, United States*

Wenbo Bao − *Department of Applied Physics and Applied Mathematics, Columbia University, New York, New York 10027, United States*

Zhihao Yang − *Department of Applied Physics and Applied Mathematics, Columbia University, New York, New York 10027, United States*

Yihan Li − *Department of Applied Physics and Applied Mathematics, Columbia University, New York, New York 10027, United States*

Yeshiyuan Zhou − *Department of Applied Physics and Applied Mathematics, Columbia University, New York, New York 10027, United States*

Zhihao Xu − *Department of Aerospace and Mechanical Engineering, University of Notre Dame, Notre Dame, Indiana 46556, United States*; orcid.org/0000-0003-1054-3669

Jinkai Si − *Department of Applied Physics and Applied Mathematics, Columbia University, New York, New York 10027, United States*

Joseph Francis Wild − *Department of Applied Physics and Applied Mathematics, Columbia University, New York, New York 10027, United States*

Complete contact information is available at: https://pubs.acs.org/10.1021/acsami.5c13443

Author Contributions

[‖]Y.Y. and T.M. contributed equally to this work.

Notes

The authors declare the following competing financial interest(s): A patent application has been filed.

ACKNOWLEDGMENTS

This work was supported by the isotope program in the Department of Energy of the United States under Grant Number DE-SC0022256 and DE-SC0024916. Y.Y. acknowledges support from the RISE award from Columbia University.

REFERENCES

(1) USDOE Office of Science (SC). *Meeting Isotope Needs and Capturing Opportunities for the Future: The 2015 Long Range Plan for the DOE-NP Isotope Progarm, NSAC Isotopes Subcommitee, July 2015*; USDOE Office of Science (SC) (United States): United States, 2015. https://www.osti.gov/biblio/1298983, https://www.osti.gov/servlets/purl/1298983.

(2) Knaster, J.; Moeslang, A.; Muroga, T. Materials research for fusion. *Nat. Phys.* **2016**, *12* (5), 424−434.

(3) Horvath, A.; Rachlew, E. Nuclear power in the 21st century: Challenges and possibilities. *Ambio* **2016**, *45* (1), 38−49.

(4) Zaret, B. L.; Wackers, F. J. Nuclear Cardiology. *N. Engl. J. Med.* **1993**, *329* (11), 775−783.

(5) Oganessian, Y. T.; Utyonkov, V. K. Superheavy nuclei from 48Ca-induced reactions. *Nucl. Phys. A* **2015**, *944*, 62−98.

(6) Oganessian, Y. T.; Yeremin, A. V.; Popeko, A. G.; Bogomolov, S. L.; Buklanov, G. V.; Chelnokov, M. L.; Chepigin, V. I.; Gikal, B. N.; Gorshkov, V. A.; Gulbekian, G. G.; et al. Synthesis of nuclei of the superheavy element 114 in reactions induced by 48Ca. *Nature* **1999**, *400* (6741), 242−245.

(7) Tang, K.; Kim, H. S.; Ramanayaka, A. N.; Simons, D. S.; Pomeroy, J. M. Targeted enrichment of 28Si thin films for quantum computing. *J. Phys. Commun.* **2020**, *4* (3), 035006.

(8) Beams, J. W.; Snoddy, L. B.; Kuhlthau, A. R. *Tests of the Theory of Isotope Separation by Centrifuging*; Virginia. Univ, 1958; Orig. Receipt Date: 31-DEC-58, https://www.osti.gov/biblio/4307544DOI:OtherInformation:PreparedfortheSecondU.N.InternationalConferenceonthePeacefulUsesofAtomicEnergy.

(9) Love, L. O. Electromagnetic Separation of Isotopes at Oak Ridge. *Science* **1973**, *182* (4110), 343−352.

(10) Graham, T. XVII. On the molecular mobility of gases. *Philos. Trans. R. Soc. London* **1863**, *153*, 385−405.

(11) Urey, H. C. The thermodynamic properties of isotopic substances. *J. Chem. Soc.* **1947**, 562−581.

(12) Letokhov, V. Laser isotope separation. *Nature* **1979**, *277* (5698), 605−610.

(13) Murray, R. L.; Holbert, K. E. *Nuclear Energy: An Introduction to the Concepts, Systems, and Applications of Nuclear Processes*; Elsevier, 2014.

(14) Betts, R. H.; Bron, J. A discussion of partial isotope separation by means of solvent extraction. *Sep. Sci.* **1977**, *12* (6), 635−639.

(15) Andreev, B. M. Separation of hydrogen isotopes in H2O-H2S system. *Sep. Sci. Technol.* **2001**, *36* (8−9), 1949−1989.

(16) Collén, B. Electrolytic Separation of Lithium Isotopes in Aqueous Solutions of Lithium Chloride Using a Mercury Cathode. *Acta Chem. Scand.* **1963**, *17*, 2410.

(17) Nishizawa, K.; Takano, T.; Ikeda, I.; Okahara, M. Extractive separation of lithium isotopes by crown ethers. *Sep. Sci. Technol.* **1988**, *23* (4−5), 333−345.

(18) Heumann, K. G.; Schiefer, H. P. Calcium isotope separation on an exchange resin having cryptand anchor groups. *Angew Chem. Int. Ed. Engl.* **1980**, *19* (5), 406−407.

(19) Knoechel, A.; Wilken, R. D. Isotopic shifts in chemical exchange systems. I. Large isotope effects in the complexation of sodium (1+) isotopes by macrocyclic polyethers. *J. Am. Chem. Soc.* **1981**, *103* (19), 5707−5711.

(20) Kim, D. W.; Kang, B. M.; Jeon, B. K.; Ryu, H. Adsorption and isotope effects by ion exchange with aqueous-2-aminomethyl-18-crown-6 bonded Merrifield resin. *J. Colloid Interface Sci.* **2002**, *254* (1), 190−194.

(21) Okuyama, K.; Okada, I.; Saito, N. The isotope effects in the isotope exchange equilibria of lithium in the amalgam-solution system. *J. Inorg. Nucl. Chem.* **1973**, *35* (8), 2883−2895.

(22) Zhang, Z.; Murali, A.; Sarswat, P. K.; Free, M. L. High-efficiency lithium isotope separation in an electrochemical system with 1-butyl-3-methylimidazolium dicyanamide, 1-ethyl-3-methylimidazolium bis (trifluoromethylsulfonyl) imide, and diethyl carbonate as the solvents. *Sep. Purif. Technol.* **2020**, *253*, 117539.

(23) Heumann, K. G. Isotopic separation in systems with crown ethers and cryptands. In *Organic Chemistry*; Springer, 2006; pp 77–132.
(24) Jones, R. C.; Furry, W. The separation of isotopes by thermal diffusion. *Rev. Mod. Phys.* **1946**, *18* (2), 151.
(25) Eyring, H.; Sherman, A. Theoretical considerations concerning the separation of isotopes. *J. Chem. Phys.* **1933**, *1* (6), 345–349.
(26) Hathorne, E. C.; James, R. H. Temporal record of lithium in seawater: a tracer for silicate weathering? *Earth Planet. Sci. Lett.* **2006**, *246* (3–4), 393–406.
(27) Misra, S.; Froelich, P. N. Lithium isotope history of Cenozoic seawater: changes in silicate weathering and reverse weathering. *science* **2012**, *335* (6070), 818–823.
(28) Bohlin, M. S.; Bickle, M. J. The reactive transport of Li as a monitor of weathering processes in kinetically limited weathering regimes. *Earth Planet. Sci. Lett.* **2019**, *511*, 233–243.
(29) Mavromatis, V.; Gautier, Q.; Bosc, O.; Schott, J. Kinetics of Mg partition and Mg stable isotope fractionation during its incorporation in calcite. *Geochim. Cosmochim. Acta* **2013**, *114*, 188–203.
(30) Saulnier, S.; Rollion-Bard, C.; Vigier, N.; Chaussidon, M. Mg isotope fractionation during calcite precipitation: an experimental study. *Geochim. Cosmochim. Acta* **2012**, *91*, 75–91.
(31) Kosmulski, M.; Jaroniec, M. Isotope exchange kinetics at heterogeneous solid surfaces (solid-liquid interfaces). *Monatsh. Chem.* **1984**, *115* (2), 147–154.
(32) Li, W.; Liu, X.-M. Experimental investigation of lithium isotope fractionation during kaolinite adsorption: Implications for chemical weathering. *Geochem. Cosmochim. Acta* **2020**, *284*, 156–172.
(33) Zhou, J.; Chen, J.; Wu, J.; Xia, S.; Zou, C. Influence of 7Li enrichment on Th-U fuel breeding performance for molten salt reactors under different neutron spectra. *Prog. Nucl. Energy* **2020**, *120*, 103213.
(34) Ishida, T.; Ono, Y. Early history of chemical exchange isotope enrichment and lessons we learn. *J. Nucl. Sci. Technol.* **2006**, *43* (4), 391–399.
(35) Bachman, J. C.; Muy, S.; Grimaud, A.; Chang, H.-H.; Pour, N.; Lux, S. F.; Paschos, O.; Maglia, F.; Lupart, S.; Lamp, P.; et al. Inorganic solid-state electrolytes for lithium batteries: mechanisms and properties governing ion conduction. *Chem. Rev.* **2016**, *116* (1), 140–162.
(36) Tanibata, N.; Kato, M.; Takimoto, S.; Takeda, H.; Nakayama, M.; Sumi, H. High formability and fast lithium diffusivity in metastable spinel chloride for rechargeable all-solid-state lithium-ion batteries. *Adv. Energy Sustain. Res.* **2020**, *1* (1), 2000025.
(37) Zhang, Y.; Squire, H.; Gurkan, B.; Maginn, E. Refined Classical Force Field for Choline Chloride and Ethylene Glycol Mixtures over Wide Composition Range. *J. Chem. Eng. Data* **2022**, *67* (8), 1864–1871.
(38) Feynman, R. P.; Hibbs, A. R.; Styer, D. F. *Quantum Mechanics and Path Integrals*; Courier Corporation, 2010.
(39) Mezei, M. THE FINITE-DIFFERENCE THERMODYNAMIC INTEGRATION, TESTED ON CALCULATING THE HYDRATION FREE-ENERGY DIFFERENCE BETWEEN ACETONE AND DIMETHYLAMINE IN WATER. *J. Chem. Phys.* **1987**, *86* (12), 7084–7088.
(40) Giannozzi, P.; Baroni, S.; Bonini, N.; Calandra, M.; Car, R.; Cavazzoni, C.; Ceresoli, D.; Chiarotti, G.; Cococcioni, M.; Dabo, I.; et al. QUANTUM ESPRESSO: a modular and open-source software project for quantum simulations of materials. *J. Phys. Condens. Matter* **2009**, *21* (39), 395502.
(41) Bagayoko, D. Understanding density functional theory (DFT) and completing it in practice. *AIP Adv.* **2014**, *4* (12), 127104.
(42) Perdew, J. P.; Burke, K.; Ernzerhof, M. Generalized gradient approximation made simple. *Phys. Rev. Lett.* **1996**, *77* (18), 3865.
(43) Baroni, S.; Giannozzi, P.; Isaev, E. Density-Functional Perturbation Theory for Quasi-Harmonic Calculations. *Rev. Mineral. Geochem.* **2010**, *71*, 39–57.
(44) Young, E. D.; Manning, C. E.; Schauble, E. A.; Shahar, A.; Macris, C. A.; Lazar, C.; Jordan, M. High-temperature equilibrium isotope fractionation of non-traditional stable isotopes: Experiments, theory, and applications. *Chem. Geol.* **2015**, *395*, 176–195.
(45) Pinilla, C.; Blanchard, M.; Balan, E.; Natarajan, S. K.; Vuilleumier, R.; Mauri, F. Equilibrium magnesium isotope fractionation between aqueous Mg2+ and carbonate minerals: Insights from path integral molecular dynamics. *Geochim. Cosmochim. Acta* **2015**, *163*, 126–139.
(46) Li, Q.; Lu, X.; Chen, M.; Zhang, L.; Cheng, Y.; Liu, X.; Yin, Z. Lithium partition and isotopic fractionation for cation exchange in clay: insights from molecular simulations. *Geochim. Cosmochim. Acta* **2023**, *358*, 148–161.
(47) Pátek, J.; Klomfar, J. Solid–liquid phase equilibrium in the systems of LiBr–H2O and LiCl–H2O. *Fluid Phase Equilib.* **2006**, *250* (1–2), 138–149.
(48) Takamoto, S.; Shinagawa, C.; Motoki, D.; Nakago, K.; Li, W.; Kurata, I.; Watanabe, T.; Yayama, Y.; Iriguchi, H.; Asano, Y.; et al. Towards universal neural network potential for material discovery applicable to arbitrary combination of 45 elements. *Nat. Commun.* **2022**, *13* (1), 2991.

https://doi.org/10.1021/acsami.5c13443
ACS Appl. Mater. Interfaces XXXX, XXX, XXX–XXX